Available online at www.sciencedirect.com
ScienceDirect
Journal of Nuclear Materials 373 (2008) 22–27
journal of nuclear materials
www.elsevier.com/locate/jnucmat

Irradiation creep and precipitation in a ferritic ODS steel under helium implantation

J. Chen [a,*], P. Jung [b], M.A. Pouchon [a], T. Rebac [a], W. Hoffelner [a]

[a] Department of Nuclear Energy and Safety, Paul Scherrer Institut, CH-5232 Villigen PSI, Switzerland
[b] Institut für Festkörperforschung, Foschungszentrum Jülich, D-52425 Jülich, Germany

Received 29 November 2006; accepted 21 April 2007

Abstract

Ferritic oxide dispersion strengthened (ODS) steel, PM2000, has been homogeneously implanted with helium under uniaxial tensile stresses from 20 to 250 MPa to maximum doses of about 0.75 dpa (3000 ppm He) with displacement damage rates of 5.5×10^{-6} dpa/s at temperatures of 573, 673 and 773 K. Straining of a miniaturized dog-bone specimen under helium implantation was monitored by linear variable displacement transformer (LVDT) and meanwhile by their resistance also measured by four-pole technique. Creep compliance was almost constant at 5.7×10^{-6} dpa^{-1} MPa^{-1} for temperatures below 673 K and increased to 18×10^{-6} dpa^{-1} MPa^{-1} at 773 K. The resistivity of PM2000 samples decreased with dose and showed a tendency to saturation. Subsequent transmission electron microscopy observations indicated the formation of ordered $Fe_{3-x}Cr_xAl$ precipitates during implantation. Correlations between the microstructure and resistivity are discussed.

1. Introduction

Operation temperatures of future advanced gas cooled reactors within the framework of the International Generation-IV-Initiative Forum [1] will exceed 1173 K with the aim to even reach 1273 K and more. This calls for creep-resistant structural materials not only for piping and heat exchangers but also for in-core or close to core supports or fixtures. Materials with high creep resistance under irradiation at very high temperatures must especially be developed. Oxide dispersion strengthened (ODS) steels may be candidates, since the nano-size oxide dispersoids act as thermodynamically stable obstacles to dislocation movement up to temperature of $T/T_m = 0.9$ [2]. Furthermore, the thermal stresses caused by temperature gradients in components made from ferritic/martensitic ODS steels can be more than three times less compared to nickel-based alloys due to their relatively high thermal conductivity and low thermal expansion coefficient [3]. These advantages add to the overall better radiation resistance of the ferritic/martensitic steels and have stimulated investigations for nuclear fission and fusion application worldwide in the last decade [4–10]. Recently, some studies on phase stability and bubble/void evolution in these steels by means of a dual-ion irradiation have been reported [5, 11–13]. Only a few experiments investigated the mechanical properties of ODS steels after irradiation, while irradiation creep data of ODS steels are rather scarce and are still missing for PM2000. Irradiation creep under simultaneous high helium production is a topic which has not yet been addressed, but may be relevant in advanced nuclear power plants. Another important concern is the microstructural stability, which can be assessed in general by measurement of electrical resistivity and in detail by analytical transmission electron microscopy (TEM). Therefore, in the present work, in situ irradiation creep of the ODS alloy PM2000, and resistivity change were investigated during He-implantation, while microstructural changes were studied by TEM after implantation.

* Corresponding author. Tel.: +41 56 310 2280; fax: +41 56 310 4595.
E-mail address: jiachao.chen@psi.ch (J. Chen).

0022-3115/$ - see front matter © 2007 Elsevier B.V. All rights reserved.
doi:10.1016/j.jnucmat.2007.04.051

2. Experimental

The ferritic ODS alloy PM2000 was supplied by Plansee GmbH in the form of 15 mm thick plates of nominal composition (wt%, balance Fe) 20% Cr, 0.5% Ti, 5.5% Al, and 0.5% Y_2O_3. The alloy was manufactured mechanically by alloying in a high energy mill, with the powder consolidated by hot compaction, followed by a hot and cold rolling procedure and a final thermal treatment [8,14] giving a quite uniform dispersion of yttria. Fig. 1 shows the metallographic cut along longitudinal direction (a), TEM micrographs of microstructure (b) and the Y_2O_3 particle size distribution from image analysis (c), of PM2000 in condition as-received. From those pictures, one can summarize that the rolling procedure produced grains with sizes of roughly $1 \times 1 \times (>12)\ mm^3$, elongated along the rolling direction. The average diameter and number density of the Y_2O_3 particles were (28 ± 8) nm and 5.1×10^{20} particles/m^3, respectively. Dog-bone shaped creep samples of 300 μm thickness were cut by spark erosion perpendicular to the rolling direction in an attempt to have at least a few grain boundaries within the gauge section. For future application of this material, thermo-mechanical treatment will need optimization. The samples were mechanical polished on both sides to 100 μm with grad 2400 paper. The final samples had an overall size of 28 mm in length, 8 mm in width and 0.1 mm in thickness, with a gauge volume of $10 \times 2 \times 0.1\ mm^3$.

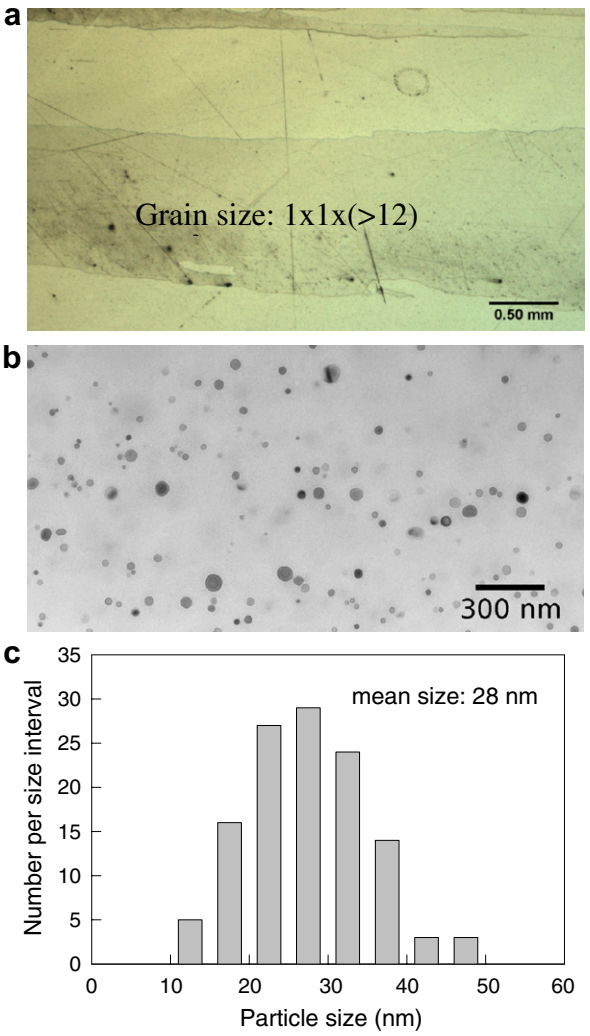

Fig. 1. Microstructure of as received PM2000 alloy, cut along longitudinal direction (a), TEM micrograph of microstructure (b), and size distribution of Y_2O_3 particles from image analysis (c).

In situ creep under He-implantation was performed at the compact cyclotron of Forschungszentrum Juelich. Details of the experimental set up are described in Ref. [15]. With 24 MeV $^4He^{2+}$ ions passing through a magnet scanning system and a degrader wheel with 24 Al-foils of variable thicknesses, the 0.1 mm thick samples were 3D-homogeneously implanted under constant uniaxial stress. Typical implantation rates were 0.023 ppm per second. The concurrent production of displacement damage was calculated by TRIM and SRIM for displacement threshold energy of 40 eV and a binding energy of 3 eV, giving per implanted He-atom 294 displacements on the front side and 194 on the back side, averaging to 244 displaced lattice atoms. With an average beam current density of 6.1 μA/cm^2, a displacement rate of about 5.5×10^{-6} dpa/s (displacements per atom per second) is derived. The irradiation creep strains were monitored by LVDT (linear variable displacement transducer) while the resistance was derived by a four-pole technique during beam-off periods. The implantation was continued until the strain rate became constant (stationary creep). Then the implantation of the same specimen was continued at a different stress in the range of 20–250 MPa. To minimize systematic errors from dose effects on the microstructure, e.g., by accumulation of irradiation defects, applied stress was changed alternatively to higher and lower values as indicated in Fig. 2. For each specimen, the temperature was fixed at 573, 673 or 773 K, respectively. The temperature distribution along the gauge region was monitored by an infrared pyrometer under 45° from the backside of the specimens. Finally, TEM specimens were prepared from the implanted gauge sections (see Ref. [16] for details) and TEM examinations were performed with a JEM 2010 at PSI.

3. Results

3.1. Irradiation creep

Fig. 2 shows the strain $\varepsilon(\sigma) = \frac{\Delta l}{l_0}$ of PM2000 during implantation as a function of the displacement dose at 573 (a), 673 (b) and 773 K (c), respectively. At all three temperatures, a contraction of the specimen against the applied tensile stress occurs at the beginning of irradiation, but already after 0.05 dpa, creep in the stress direction is observed. Each stress change caused, aside from elastic strain, also a short transient stage before stationary creep was reached. Those transient strains are similar to observations in other materials [17] and are ascribed to

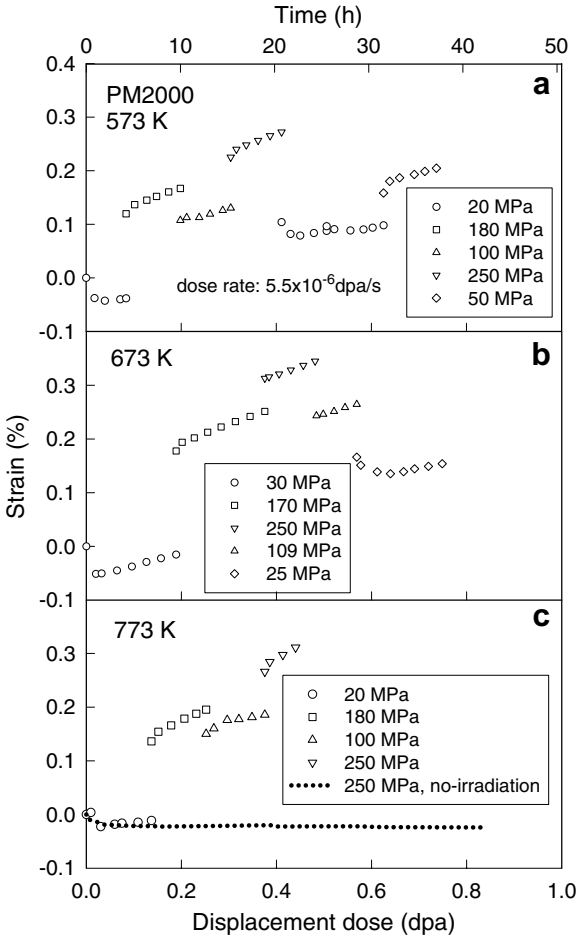

Fig. 2. Strain of PM2000 during He-implantation at 573 (a), 673 (b) and 773 K (c) as a function of displacement dose at different stresses.

irradiation-induced relaxation. For comparison, thermal creep as a function of time (upper abscissa, corresponding to time at a dose rate of 5.5×10^{-6} dpa/s) at 773 K under 250 MPa is included in Fig. 2(c). A short contraction is observed at the very beginning, similar to the irradiation case, but no measurable stationary straining. This demonstrates that in PM2000 thermal creep is negligible even at 773 K. Irradiation-induced creep rates, ε', i.e. strain-rate per dose-rate (in unit of dpa^{-1}) were obtained by fitting straight lines to the stationary parts of the curves in Fig. 2. These values are plotted in Fig. 3 as a function of the applied stress for all three implantation temperatures (stationary creep was not reached at 250 MPa in the 773 K irradiation due to a cyclotron shut-down). The data can be fitted by linear stress dependence up to 250 MPa (solid line):

$$\varepsilon'(\sigma) = B_0 \cdot \sigma + \varepsilon'_0 \tag{1}$$

with creep compliances B_0, i.e., creep rate per dose rate (assuming linear dependence) and stress, of $5.7\times10^{-6}\,\text{dpa}^{-1}\,\text{MPa}^{-1}$ and $18\times10^{-6}\,\text{dpa}^{-1}\,\text{MPa}^{-1}$ at temperatures of $\leqslant$673 K and 773 K, respectively. Extrapolating the lines in Fig. 3 to zero stress gives ordinate-offsets ε'_0

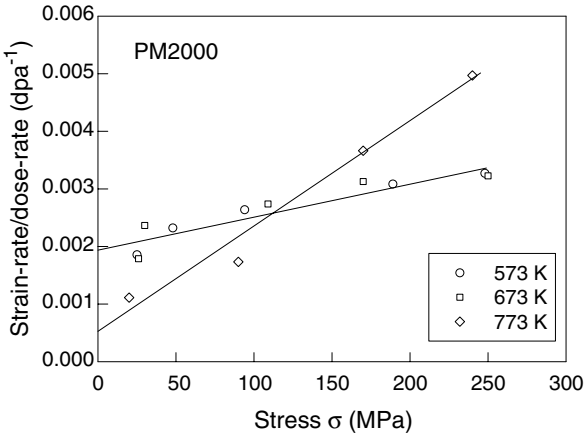

Fig. 3. Irradiation creep rates per displacement rates of PM2000 as a function of tensile stress under He-implantation at 573, 673 and 773 K. Solid lines are linear fits to determine irradiation creep compliances.

of 1.96×10^{-3} and 4.9×10^{-4} dpa^{-1} at temperatures of $\leqslant$673 and 773 K, respectively. ε'_0 represents stress-independent dimensional changes, for example from volume swelling:

$$\frac{\Delta V}{V} = 3\cdot\varepsilon'_0. \tag{2}$$

3.2. Resistivity and TEM observation

The resistivity of PM2000 has a very small temperature dependence, the difference between 25 °C and 500 °C being less than 0.5%. This means that temperature is not a critical issue for precise resistance measurements. During irradiation the resistance measurements were performed after switching off the α-beam and waiting for 12 min to stabilise near room temperature. As these measurements were performed under various stresses, the resistance values have to be corrected for effects of elastic strains on specimen geometry, using resistance–stress relations measured before irradiation, assuming that irradiation does not change these relations. These corrections amount to less than 0.3% and were therefore neglected. Thermal creep and aging experiments were performed at a constant stress of 250 MPa at 773 K and 0 MPa at 673 K, respectively. The resistance was measured at creep temperature on the 773 K specimen and at room temperature on the 673 K specimen. These measurements showed only a minor decrease of resistivity, while a significant decrease of resistivity is observed under implantation/irradiation. In Fig. 4, the evolution of electrical resistivity during irradiation (symbols) and thermal aging (dotted line) is compared. Stress changes in both directions cause increase in resistivity, most significantly when stress is decreased to 25 and 26 MPa in the 573 K and 673 K specimens, respectively.

A decrease in resistivity under irradiation is an unspecific indication of microstructural changes. Therefore TEM was conducted on un-implanted and implanted

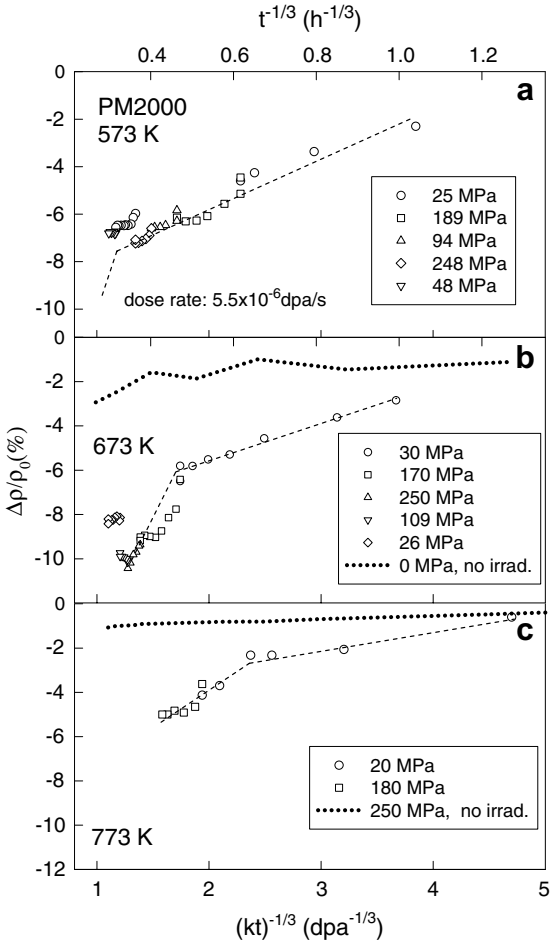

Fig. 4. Relative changes of electrical resistivity of PM 2000 during He-implantation at 573 (a), 673 (b) and 773 K (c) at indicated stresses. Doted lines in (b) and (c) refer to thermal aging without stress at 673 K and thermal creep at 773 K, respectively. Resistance was measured at room temperature, except for thermal creep, where measurements were taken during test at 773 K.

specimens. Fig. 5 shows a TEM dark field image of a sample after an irradiation creep test at 673 K, using a $(3\bar{1}1)$ superlattice reflection, marked by the arrow in the inserted diffraction pattern which was taken along the [1 1 0] zone axis. By further analysis of the diffraction pattern, the structure was identified as $D0_3$ and ascribed to the ordered precipitate $Fe_{3-x}Cr_x$ Al. From the dark-field image, an average size of 3.6 nm, a particle density of $3\times10^{23}/m^3$, and a volume fraction of 0.9% are derived. No evidence of such $Fe_{3-x}Cr_x$ Al precipitates was detected in other specimens, neither in the as-received or thermally crept and aged samples, nor in the irradiation creep samples from implantations at 573 K and 773 K. A detailed report on microstructural changes after He-implantation will be given elsewhere.

4. Discussion

The temperature-dependence of creep strain rates with and without He-implantation [18] is given in Fig. 6. The

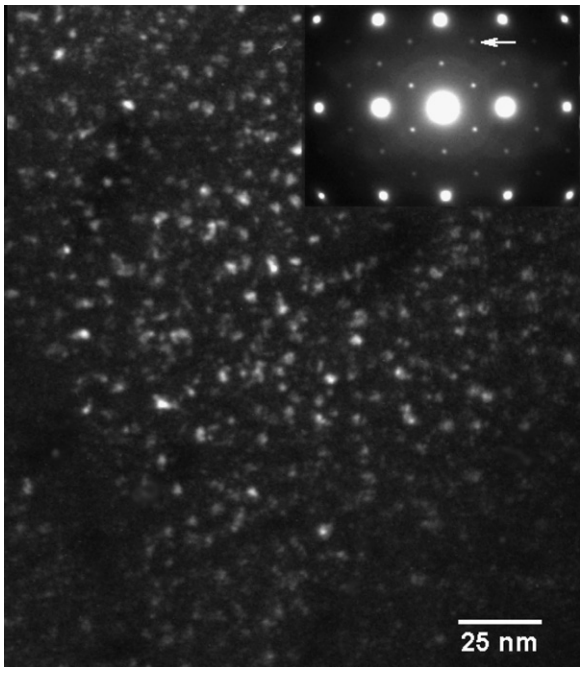

Fig. 5. TEM dark field image after irradiation creep test at 673 K, taken by a $(3\bar{1}1)$ superlattice reflection (indicated by the arrow on the inserted diffraction pattern) along the [1 1 0] zone axis.

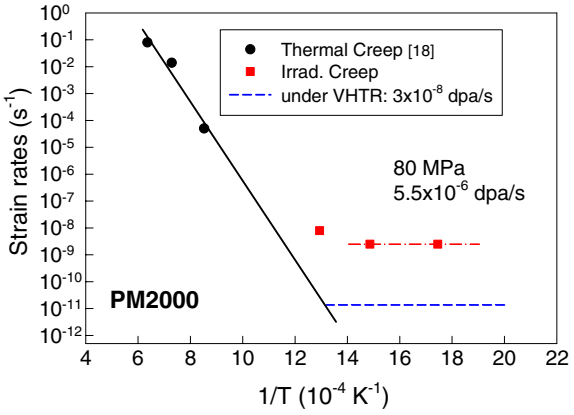

Fig. 6. Temperature dependence of creep rates of PM2000 without irradiation (solid line), under He-implantation (dash-dotted), and expected for VHTR conditions (dashed line).

thermal creep data are from standard bulk specimens [18]. The effect of miniature size of the present specimens on creep cannot be precisely assessed, as the literature on this topic is contradictory [19,20]. Expected creep rates under conditions in future, very high temperature reactors (VHTR) are included. The present data show that the irradiation creep rate of PM2000 is the same for 573 K and for 673 K. Extrapolation of irradiation data at 80 MPa and 3×10^{-8} dpa/s match the thermal creep line at about 760 K. According to earlier experimental findings [21–23] and theoretical understanding [24,25], irradiation creep dominates at low temperatures when the thermal vacancy concentration is negligible. Only a minor temperature dependence is expected in this area. When thermal creep

dominates at high temperatures, irradiation will have no major influence on creep rates [22] except possibly via irradiation induced microstructural or compositional changes.

The volume change $\Delta V/V$ (5.9×10^{-3}/dpa at $\leqslant$673 K) derived from the offset value ε_0' is more than one order of magnitude above typical swelling in reactor irradiated ferritic steels. On the other hand, a comparison to the amount of implanted helium (using the above value of 244 dpa/He) gives a reasonable volume change of 0.48 atomic volumes per He-atom.

Small increase of resistivity, uniformly after stress changes in both directions, have been reported previously [17] and may be caused by detrapping of defects or clusters from dislocations (Cottrell clouds), if the resistivity of attached defects is smaller than that of separated ones (non-linear superposition). An increase of resistivity caused by retention of displacement defects will not exceed about 1%/dpa [26], due to defect saturation, i.e., less than +0.75% in the present case. On the other hand, segregation or precipitation can decrease the resistivity, due to solute depletion in the matrix or due to ordering. In Fig. 4, the electrical resistivity data were plotted for a $(kt)^{-1/3}$ dose dependence (k is damage rate, t is time), which is expected for diffusion controlled growth of precipitates [27–29]. The results in Fig. 4 suggest a two-stage process, the first of which roughly conforms to a $(kt)^{-1/3}$ behaviour. This can be ascribed to decomposition of the original Fe(Al) solution of concentration c_{Al} (=11.4 at.%) into a volume fraction υ_s of Al-concentration c_s and a depleted matrix of c'_{Al}. For negligible change of atomic density, conservation of the Al content yields:

$$(1-\upsilon_s)\cdot c'_{Al}+\upsilon_s\cdot c_s=c_{Al}. \tag{3}$$

An upper limit of c_s of 25 at.% is given by the atomic concentration of the Fe_3Al phase. Resistivities of depleted matrix and of enriched areas are given by

$$\rho'_M=\rho_0+r_{Al}\cdot(c'_{Al}-c_{Al}) \tag{4}$$

and

$$\rho_s=\rho_0+r_{Al}\cdot(c_s-c_{Al}), \tag{5}$$

where $\rho_0=1.78\times10^{-6}\,\Omega$m is the resistivity of the original solute, and $r_{Al}=6.4\times10^{-6}\,\Omega$m/uc [30] is the resistivity change of iron per unit concentration of Al. For cube-shaped geometry of the enriched areas, the resulting total resistivity is given by [31]

$$\rho'=\frac{\rho'_M}{x+1}\cdot\frac{\rho'_M\cdot x+\rho_p\cdot\frac{x^3+2x^2+3x+1}{x(x+1)}}{\rho'_M\cdot x+\rho_p\cdot\frac{2x+1}{x}} \tag{6}$$

with $x=\frac{\upsilon_s^{1/3}}{1-\upsilon_s^{1/3}}$. By inserting an experimental value $\rho'\approx0.94\cdot\rho_0$ (at 673 K) into Eqs. (3)–(6), the parameters $\upsilon_s=0.274$, $\rho'_M=1.45\cdot10^{-6}\,\Omega$m, and $c'_{Al}=6.27$ at.% are derived. For a smaller value of $c_s=0.2$, the respective results would be 0.45, $1.33\times10^{-6}\,\Omega$m, and 4.4 at.%. Very similar results were obtained when instead of Eq. (6), the two contributions ρ'_M and ρ_s are simply set parallel: $\frac{1}{\rho'}=\frac{1-\upsilon_s}{\rho_M}+\frac{\upsilon_s}{\rho_s}$.

The second stage in Fig. 4 (not reached at 573 K) is then ascribed to formation of a volume fraction $\upsilon_p=0.9\%$ (at 673 K from TEM) of ordered Fe_3Al ($c_p=25$ at.%) in the enriched areas. Using parallel circuiting of the three contributions gives:

$$\frac{1}{\rho''}\approx\frac{\upsilon_p}{\rho_p}+\frac{\upsilon_s-\upsilon_p}{\rho_s}+\frac{1-\upsilon_s}{\rho'_M} \tag{7}$$

with the experimental value $\rho''\approx0.9\cdot\rho_0$ (at 673 K) from Fig. 3(b) one obtain $\rho_p=0.374\times10^{-6}\,\Omega$m. As the resistivity of pure Fe_3Al is not available, ρ_p must be compared to pure iron $\rho_{Fe}=0.103\times10^{-6}\,\Omega$m, which certainly is a lower limit for ρ_p. The difference between ρ_p and ρ_{Fe} is ascribed to some Cr content in $Fe_{3-x}Cr_xAl$, which is limited to less than 5 at.%, i.e., $x\leqslant0.15$, due to $r_{Cr}=4.7\times10^{-6}$ Ωm/uc [28]. It should be noted that $\rho_{Fe}+c_{Cr}\cdot r_{Cr}+c_{Al}\cdot r_{Al}$ closely approaches ρ_0, with the rest accounted for by Ti and Y_2O_3. The above analysis only refers to 673 K, where superlattice reflexions were observed. At 573 K slow diffusion and at 773 K disordering by thermal effects may cause a smaller size of the precipitates and/or their less complete ordering both of which prevent observation of superlattice reflexions. According to the Fe–Al phase diagram [32,33] ordered Fe_3Al precipitates between 12 wt% and 20 wt% Al at temperatures below 823 K (it was also reported that ordered Fe_3Al exists at least up to 1000 K [34]). Two explanations are possible for the present observation of Fe_3Al which has never been reported before in the Fe–Cr–Al system with an Al content of 5.5 wt% (below the solubility limit of 12 wt%). One is that irradiation-enhanced diffusion promotes phase equilibria in alloys where thermal diffusion becomes exceedingly slow at low temperature (then the phase diagram should be revised) [35]. The other explanation is, that the presence of non-equilibrium point defects during irradiation affects the free energies of phases and therefore shifts the solubility [35]. The stability of precipitation under irradiation and their effect on mechanical behaviour deserves further detailed investigation.

5. Summary

(1) Irradiation creep rates of PM2000 show linear stress dependence up to 250 MPa at temperatures from 573 K to 773 K.
(2) Irradiation creep rate per dose rate and stress is almost constant at temperatures below 673 K and somewhat increases at 773 K, while at even higher temperatures as expected in future Generation-IV reactors, deformation will be dominated by thermal creep.
(3) The resistivity of PM2000 samples decreases with increasing displacement dose, which is ascribed to formation of ordered $Fe_{3-x}Cr_xAl$, as revealed by TEM observation.

Acknowledgements

The authors are grateful to H. Klein, L. Kasterke, and B. Olefs for operation of the cyclotron. Work was performed within the Swiss Generation IV Program. It was partially financed by EU-Projects EXTREMAT and RAPHAEL.

References

[1] A Technology Roadmap for Generation IV Nuclear Energy System, Issued by the US DOE Nuclear Energy Research Advisory Committee and the Generation IV International Forum, GIF-002-00, December 2002.
[2] E. Arzt, Acta Metal. Mater. 46 (1998) 5611.
[3] J. Chen, G.S. Bauer, T. Broome, F. Carsughi, Y. Dai, S.A. Maloy, M. Roedig, W.F. Sommer, H. Ullmaier, J. Nucl. Mater. 318 (2003) 56.
[4] S. Ukai, M. Fujiwara, J. Nucl. Mater. 307–311 (2002) 749.
[5] H. Kishimoto, K. Yutani, R. Kasada, A. Kimura, Fus. Eng. Des. 81 (2006) 1045.
[6] A. Alamo, H. Regle, G. Pons, L.L. Bechade, Mater. Sci. Forum 88–90 (1992) 183.
[7] M. Klimiankou, R. Lindau, A. Moeslang, J. Schroeder, Powder Metall. 48 (2005) 277.
[8] A. Czyrska-Filemonowicz, B. Dubiel, Mater. Proc. Technol. 63 (1997) 53.
[9] D.K. Mukhopadhyay, F.H. Froes, D.S. Gelles, J. Nucl. Mater. 258–263 (1998) 1209.
[10] R.L. Klueh, J.P. Shingledecker, R.W. Swindeman, D.T. Hoelzer, J. Nucl. Mater. 341 (1998) 103.
[11] T.R. Allen, J. Gan, J.I. Cole, S. Ukai, S. Shutthanandan, S. Thevuthasan, Nucl. Sci. Eng. 151 (2005) 305.
[12] E.A. Little, D.J. Mazey, W. Hanks, Scripta Metal. Mater. 25 (1991) 1115.
[13] I.-S. Kim, J.D. Hunn, N. Hashimoto, D.L. Larson, P.J. Maziasz, K. Miyahara, E.H. Lee, J. Nucl. Mater. 280 (2000) 264.
[14] Dispersion-Strengthened High-Temperature Materials, Material properties and applications, Prospectus from Plansee (2003), 706 DE.04.03(1000)RWF.
[15] P. Jung, A. Schwarz, H.K. Sahu, Nucl. Instrum. and Meth. A 234 (1985) 331.
[16] J. Chen, P. Jung, M. Nazmy, W. Hoffelner, J. Nucl. Mater. 352 (2006) 36.
[17] P. Jung, P.B. Chilson, J. Nucl. Mater. 149 (1987) 1.
[18] J. Wunder, in: Mikrostrukturelle Beschreibung der Warmfestigkeit ferritischer Superlegierungen Fortschr. –Ber. VDI Reihe 5 Nr. 510, VDI Verlag, Duesseldorf, 1997, p. 84.
[19] N. Igata, K. Miyahara, C. Tada, D. Blasl, G. Lucas, Radiat. Eff. Def. 101 (1986) 131.
[20] D.G. Rickerby, P. Fenici, P. Jung, G. Piatti, P. Schiller, ASTM–STP 888 (1986) 220.
[21] P. Jung, M.I. Ansari, J. Nucl. Mater. 138 (1986) 40.
[22] P. Jung, N.M. Afify, J. Nucl. Mater. 155–157 (1988) 1019.
[23] P. Jung, C. Schwaiger, H. Ullmaier, J. Nucl. Mater. 85 (1979) 867.
[24] H. Ullmaier, W. SchillingRadiation Damage in Metallic Reactor Materials in Physics of Modern Materials, vol. 1, International Atomic Energy Agency, Vienna, 1980, p. 301.
[25] L.K. Mansur, in: G.R. Freeman (Ed.), Kinetics of Non-homogeneous Processes, Wiley-Interscience, New York, 1987.
[26] Zh. Zhu, P. Jung, H. Klein, J. Nucl. Mater. 202 (1993) 222.
[27] K. Binder, D. Stauffer, Z. Phys. B 24 (1976) 407.
[28] I.M. Lifshitz, V.V. Slyozov, J. Phys. Chem. Sol. 19 (1961) 35.
[29] C. Wagner, Z. Elektrochem. 65 (1961) 581.
[30] J. Bass, in: Landolt–BörnsteinNew Series Group III, vol. 15a, Springer, Berlin, 1982, p. 1.
[31] T.W. Barbee Jr., R.A. Huggins, W.A. Little, Philos. Mag. 14 (1966) 255.
[32] G.V. Raynor, V.G. Rivlin, Phase Equilibria in Iron Ternary Alloys, The Institute of Metals, London, 1988, p. 10.
[33] ASM Handbook, vol. 3, Alloy Phase Diagrams, 2002.
[34] H. Kleykamp, H. Glasbrenner, Z. Metallkd. 88 (1997) 230.
[35] F.V. Nolfi (Ed.), Phase Transformations during Irradiation, Applied Science Publishers, London and New York, 1983.